A persistent ultraviolet outflow from an accreting neutron star binary transient

Castro Segura, N.; Knigge, C.; Long, K. S.; Altamirano, D.; Armas Padilla, M.; Bailyn, C.; Buckley, D. A. H.; Buisson, D. J. K.; Casares, J.; Charles, P.

[Link to publication in University of Groningen/UMCG research database](#)

Citation for published version (APA):
Castro Segura, N., Knigge, C., Long, K. S., Altamirano, D., Armas Padilla, M., Bailyn, C., Buckley, D. A. H., Buisson, D. J. K., Casares, J., Charles, P., Combi, J. A., Cúneo, V. A., Degenaar, N. D., del Palacio, S., Díaz Trigo, M., Fender, R., Gandhi, P., Georganti, M., Gutiérrez, C., ... Wiseman, P. (2022). A persistent ultraviolet outflow from an accreting neutron star binary transient. *Nature, 603*, 52-57. https://doi.org/10.1038/s41586-021-04324-2

Article

A persistent ultraviolet outflow from an accreting neutron star binary transient

N. Castro Segura[1✉], C. Knigge[1], K. S. Long[2,3], D. Altamirano[1], M. Armas Padilla[4,5], C. Bailyn[6], D. A. H. Buckley[7], D. J. K. Buisson[1], J. Casares[4,5], P. Charles[1], J. A. Combi[8], V. A. Cúneo[4,5], N. D. Degenaar[9], S. del Palacio[8], M. Díaz Trigo[10], R. Fender[11], P. Gandhi[1], M. Georganti[1], C. Gutiérrez[1,12,13], J. V. Hernandez Santisteban[14], F. Jiménez-Ibarra[15,16], J. Matthews[17], M. Méndez[18], M. Middleton[1], T. Muñoz-Darias[4,5], M. Özbey Arabacı[1], M. Pahari[1,19], L. Rhodes[11], T. D. Russell[9,20], S. Scaringi[21], J. van den Eijnden[9,11], G. Vasilopoulos[6,22], F. M. Vincentelli[1] & P. Wiseman[1]

All disc-accreting astrophysical objects produce powerful disc winds. In compact binaries containing neutron stars or black holes, accretion often takes place during violent outbursts. The main disc wind signatures during these eruptions are blue-shifted X-ray absorption lines, which are preferentially seen in disc-dominated 'soft states'[1,2]. By contrast, optical wind-formed lines have recently been detected in 'hard states', when a hot corona dominates the luminosity[3]. The relationship between these signatures is unknown, and no erupting system has as yet revealed wind-formed lines between the X-ray and optical bands, despite the many strong resonance transitions in this ultraviolet (UV) region[4]. Here we report that the transient neutron star binary Swift J1858.6-0814 exhibits wind-formed, blue-shifted absorption lines associated with C IV, N V and He II in time-resolved UV spectroscopy during a luminous hard state, which we interpret as a warm, moderately ionized outflow component in this state. Simultaneously observed optical lines also display transient blue-shifted absorption. Decomposing the UV data into constant and variable components, the blue-shifted absorption is associated with the former. This implies that the outflow is not associated with the luminous flares in the data. The joint presence of UV and optical wind features reveals a multi-phase and/or spatially stratified evaporative outflow from the outer disc[5]. This type of persistent mass loss across all accretion states has been predicted by radiation–hydrodynamic simulations[6] and helps to explain the shorter-than-expected duration of outbursts[7].

In October 2018, the Neil Gehrels Swift Observatory (Swift[8]) detected a bright new X-ray binary transient, Swift J1858.6−0814 (hereafter J1858)[9]. Multi-wavelength observations quickly led to the discovery of radio, optical and near-ultraviolet (UV) counterparts[10–12]. The detection of thermonuclear runaway explosions in X-rays (type I X-ray bursts) established that the accreting object is a neutron star located at a distance of about 13 kpc (ref. [13]). The system was also found to undergo eclipses, implying a nearly edge-on viewing angle with respect to the disc ($i \gtrsim 70°$) and revealing the orbital period to be $P_{orb} \simeq 21.3$ h(ref. [14]).

J1858 displayed extreme variability during its outburst in all energy bands, with the X-ray luminosity changing by one to two orders of magnitude on time scales of seconds (Fig. 1a)[11,14]. The X-ray spectrum consisted of a heavily absorbed thermal accretion disc component plus a very shallow non-thermal power-law tail (photon flux $N_{ph}(E) \propto E^{-\Gamma}$, with $\Gamma < 1$; where E is the energy and Γ is the spectral index)[15]. Both the peculiar X-ray spectrum and spectacular variability are reminiscent of those seen during the outbursts of the well-studied black-hole X-ray binaries V404 Cyg and V4641 Sgr, which

[1]Department of Physics & Astronomy, University of Southampton, Southampton, UK. [2]Space Telescope Science Institute, Baltimore, MD, USA. [3]Eureka Scientific, Inc., Oakland, CA, USA. [4]Instituto de Astrofísica de Canarias, La Laguna, Tenerife, Spain. [5]Departamento de Astrofísica, Universidad de La Laguna, La Laguna, Tenerife, Spain. [6]Department of Astronomy, Yale University, New Haven, CT, USA. [7]South African Astronomical Observatory, Cape Town, South Africa. [8]Instituto Argentino de Radioastronoma (CONICET; CICPBA; UNLP), Villa Elisa, Argentina. [9]Anton Pannekoek Institute for Astronomy, University of Amsterdam, Amsterdam, The Netherlands. [10]ESO, Garching bei München, Germany. [11]Astrophysics, Department of Physics, University of Oxford, Oxford, UK. [12]Finnish Centre for Astronomy with ESO (FINCA), University of Turku, Turku, Finland. [13]Tuorla Observatory, Department of Physics and Astronomy, University of Turku, Turku, Finland. [14]SUPA School of Physics & Astronomy, University of St Andrews, St Andrews, UK. [15]Department of Physics and Astronomy, Macquarie University, Sydney, New South Wales, Australia. [16]Research Centre in Astronomy, Astrophysics and Astrophotonics, Macquarie University, Sydney, New South Wales, Australia. [17]Institute of Astronomy, University of Cambridge, Cambridge, UK. [18]Kapteyn Astronomical Institute, University of Groningen, Groningen, The Netherlands. [19]Department of Physics, IIT Hyderabad, Hyderabad, India. [20]INAF, Istituto di Astrofisica Spaziale e Fisica Cosmica, Palermo, Italy. [21]Centre for Extragalactic Astronomy, Department of Physics, Durham University, Durham, UK. [22]Université de Strasbourg, CNRS, Observatoire Astronomique de Strasbourg, UMR 7550, Strasbourg, France. ✉e-mail: N.Castro-Segura@soton.ac.uk
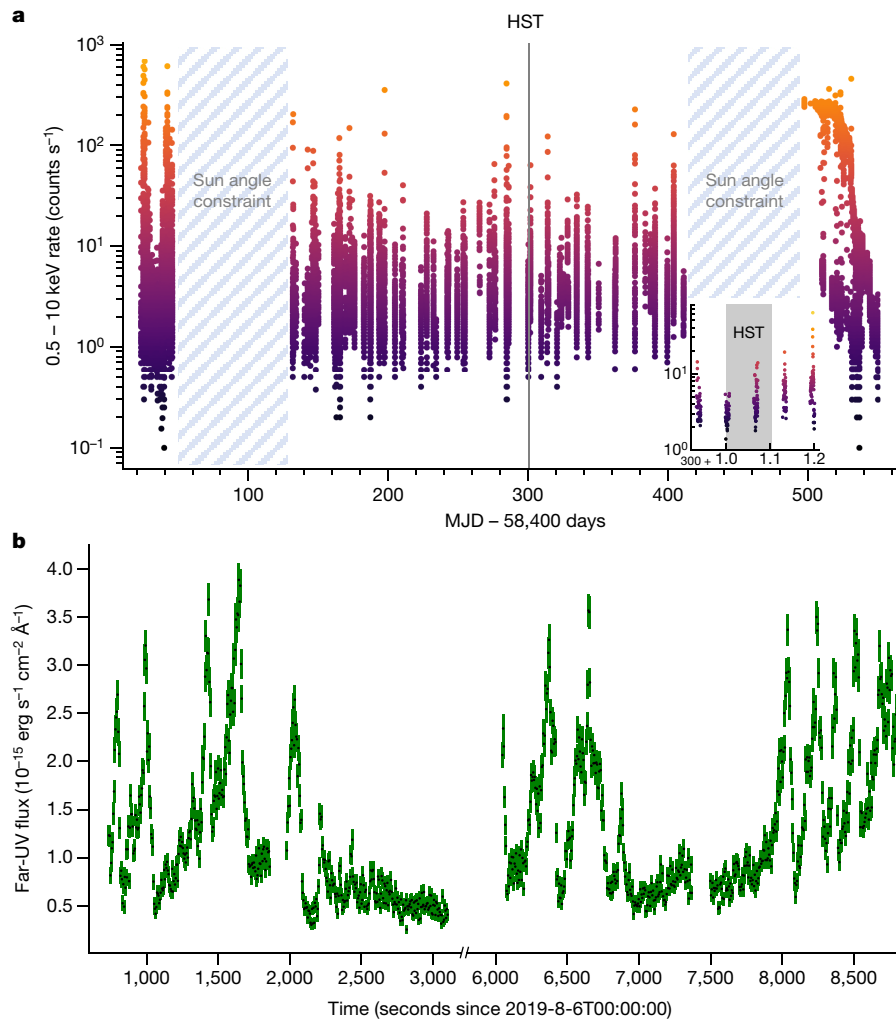
Fig. 1 | Overview light curves of the X-ray transient Swift J1858.6−0814.
a, Outburst evolution as observed with NICER in the 0.5–10 keV band
(reproduced with permission from ref.[14]); the two large gaps are caused by Sun
constraints. The source exhibits flares that reach the Eddington limit during
the first 450 days while it is in the hard state. The time of the HST far-UV
observations is marked with a vertical line. The colour code refers to the
observed count rate, covering approximately 10^{-1} counts per second (in dark
blue) to 10^3 counts per second (in light orange). Inset, an enlargement around
the time of the HST observations (at Modified Julian Date (MJD) approximately
58,701), indicated with the shaded area. The inset covers the region around the
time of the HST visit. **b**, HST far-UV light curve in 5-s bins, showing strong flares
(up to a factor of 10 increase in flux) and flickering at lower flux levels. Green
bars represent the standard error and means are indicated with small black
dots.

are thought to be a consequence of accretion at super-Eddington
rates[16,17].

To shed light on the accretion and outflow processes associated
with the outburst, we carried out strictly simultaneous, time-resolved
observations across the electromagnetic spectrum on 6 August 2019
around 00:00 (UTC). One of our primary goals was to search for
outflow signatures in the far-ultraviolet (far-UV) band, because this
region contains several strong resonance lines that are very sensi-
tive to the presence of warm, moderately ionized intervening mate-
rial. Therefore, the timing of this campaign was centred on far-UV
spectroscopic observations with the Hubble Space Telescope (HST).
Simultaneous optical spectroscopy was obtained at both the Very
Large Telescope (VLT) array and the Gran Telescopio de Canarias
(GTC). Additional information about the campaign is provided in
the Methods.

In line with data obtained at other wavelengths[11,18], the far-UV light
curve exhibits dramatic flaring activity (Fig. 1b). The X-ray, far-UV
and optical variability are clearly correlated, with any lags between
these time series being ≲3 s (F.M.V. et al., manuscript in preparation).
In agreement with previously reported X-ray light curves[13,14], there is

no evidence of thermonuclear runaway events during the campaign.
This suggests that the multi-wavelength flaring is driven by a variable
central X-ray source.

The presence of a large, strongly irradiated accretion disc is the
key requirement for a thermally driven outflow[19–21] and high incli-
nations tend to strengthen wind-formed absorption features[1,6]. All
of this makes J1858 an ideal candidate for displaying clear obser-
vational outflow signatures. As summarized in the Methods, X-ray
spectroscopy of the source obtained earlier in the same outburst
already found tentative evidence for an outflow[22]. Time-resolved
optical spectroscopy also revealed clear, but highly variable P Cygni
wind features in Hα and He I 5,876 Å during the bright hard state[3]
(Fig. 2).

Figure 3 shows the time-averaged far-UV spectrum we obtained
with HST in the hard state. The spectrum is rich in both absorption
and emission lines that span a wide range of ionization states. Most
of the low-ionization absorption lines are centred at or near the rest
wavelength of the relevant transition, with most of these lines not
being intrinsic to the system but due to interstellar absorption along
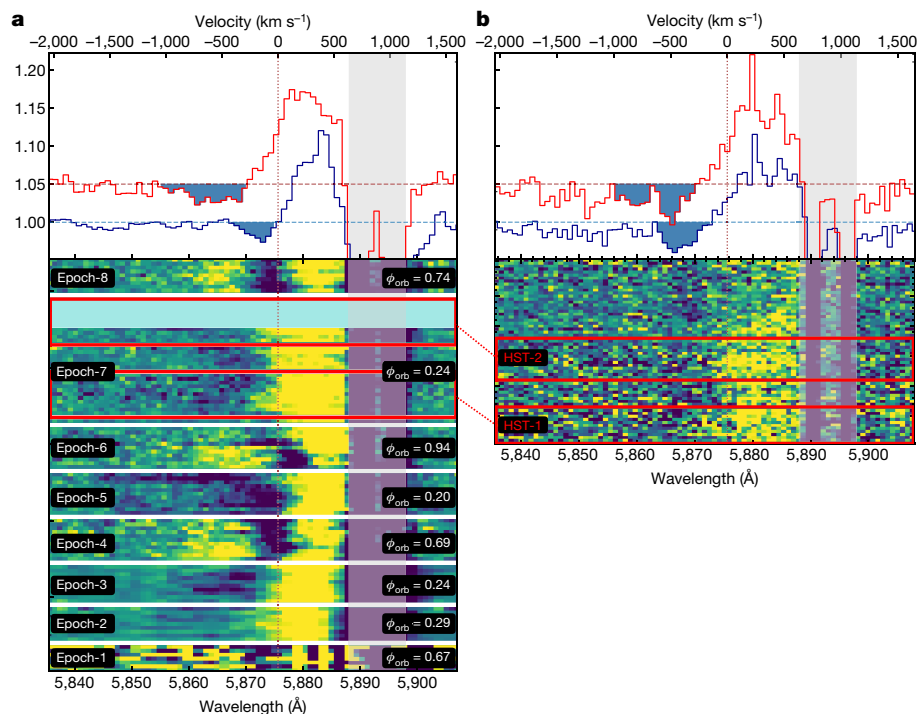the line of sight. However, at least two emission lines, N v 1,240 Å

Fig. 2 | Apparently transient optical wind signatures. a, Trailed spectra of the eight GTC/OSIRIS epochs published in ref. [3] with the corresponding orbital phase[14]. **b**, VLT/X-Shooter during the HST visit centred on He I 5,876 Å. The average spectrum of all the observations is shown in the top panel with a blue line. Strictly simultaneous observations during the two UV exposures are highlighted in red boxes, with their corresponding averaged spectrum shown in red in the top panels with a 5% offset for clarity. Absorption troughs below continuum levels are highlighted with a shaded area. The telluric absorption region around $\lambda 5,836$ Å is indicated with the shaded vertical band.

and C IV 1,550 Å, show clear evidence for associated blue-shifted absorption. As these species are associated with temperatures T of around a few 10^4 K, their presence unambiguously establishes the existence of a warm and moderately ionized outflowing component.

Several other transitions, for example, O V 1,370 Å and Si III 1,440 Å, also show tentative evidence for blue-shifted absorption. Moreover, all strong emission lines in the spectrum, which includes the Si IV 1,400 Å doublet resonance line and the He II 1,640 Å recombination feature, show evidence for a slight red-shift or a red-skew, suggesting that they are also affected by blue-shifted wind absorption.

As shown in the insets of Fig. 3, the blue edges of the far-UV absorption features extend up to $\simeq-2,000$ km s^{-1}, similar to the wind speed inferred from the optical data. However, the far-UV absorption troughs are considerably deeper than those in the optical, which rarely fall below 90–95% of the continuum. This is probably because most of the strong far-UV lines are associated with strongly scattering resonance transitions, whereas the optical features are associated with recombination lines that connect two excited levels. Very high (column) densities are required in order for such recombination lines to produce absorption. However, sensitivity of far-UV resonance lines to intervening material makes this waveband particularly valuable for studying outflows.

It is important to establish if the far-UV wind signatures are always present or are instead associated with the strong flaring events in the light curve. We have therefore carried out a maximum likelihood linear decomposition of the time-resolved spectroscopy into a constant and a flaring (variable) component. The spectra inferred for the two components are shown in Fig. 4; details regarding the decomposition technique are provided in the Methods. In both N V 1,240 Å and C IV 1,550 Å, the blue-shifted absorption signature is clearly associated with the constant component. This suggests that either our line of sight to the emitting region responsible for the flaring component

does not pass through the warm outflow or that the ionization state of the outflow changes significantly during the flares. Perhaps more importantly, it also suggests that the outflow is, in fact, always present, but that its signatures may sometimes be swamped by the flaring component (in which these signatures are absent). The same effect may be responsible for the transience of the blue-shifted absorption seen in the optical data, especially considering how weak these features are (compare with Fig. 2).

The presence of detectable blue-shifted absorption associated with the UV resonance lines (for example, N V 1,240 Å, C IV 1,550 Å) implies that the optical depth in these transitions must be significant. This, in turn, requires minimum column densities for the relevant ions, which can be cast as approximate lower limits on the mass-loss rate carried away by the outflow ($\dot{M}_{wind}$; see Methods for details). Conservatively assuming ionization fractions of $f = 1$ for both C^{3+} and N^{4+}, the limits are $\dot{M}_{wind} \gtrsim 2 \times 10^{-11}\ M_{\odot}\ yr^{-1}$ for N V 1,240 Å and $\dot{M}_{wind} \gtrsim 3 \times 10^{-12}\ M_{\odot}\ yr^{-1}$ for C IV 1,550 Å. The actual ionization fractions may be considerably lower, and the mass-loss rate correspondingly higher.

The apparent time-averaged X-ray luminosity during the flaring hard state in which we observed J1858 was $L_X \simeq 0.01L_{Edd}$, where L_{Edd} is the Eddington luminosity, although individual flares appear to have reached super-Eddington levels[13]. Taken at face value, this corresponds to an average accretion rate in this state of $\dot{M}_{acc} \simeq 10^{-10}\ M_{\odot}\ yr^{-1}$. In this case, $\dot{M}_{wind}/\dot{M}_{acc} \gtrsim 0.2$, suggesting that the wind is dynamically important and could significantly affect the accretion flow[23,24], but also see ref. [25]. However, it is also possible that the intrinsic luminosity was much higher throughout this state, with time-variable obscuration being responsible for the reduction in the time-averaged flux (and perhaps also the flaring activity). Such obscuration need not necessarily be associated with the disk wind itself (Methods).

In the extreme case that $L \simeq L_{Edd}$, the constraint on the wind efficiency is $\dot{M}_{wind}/\dot{M}_{acc} \gtrsim 10^{-3}$.
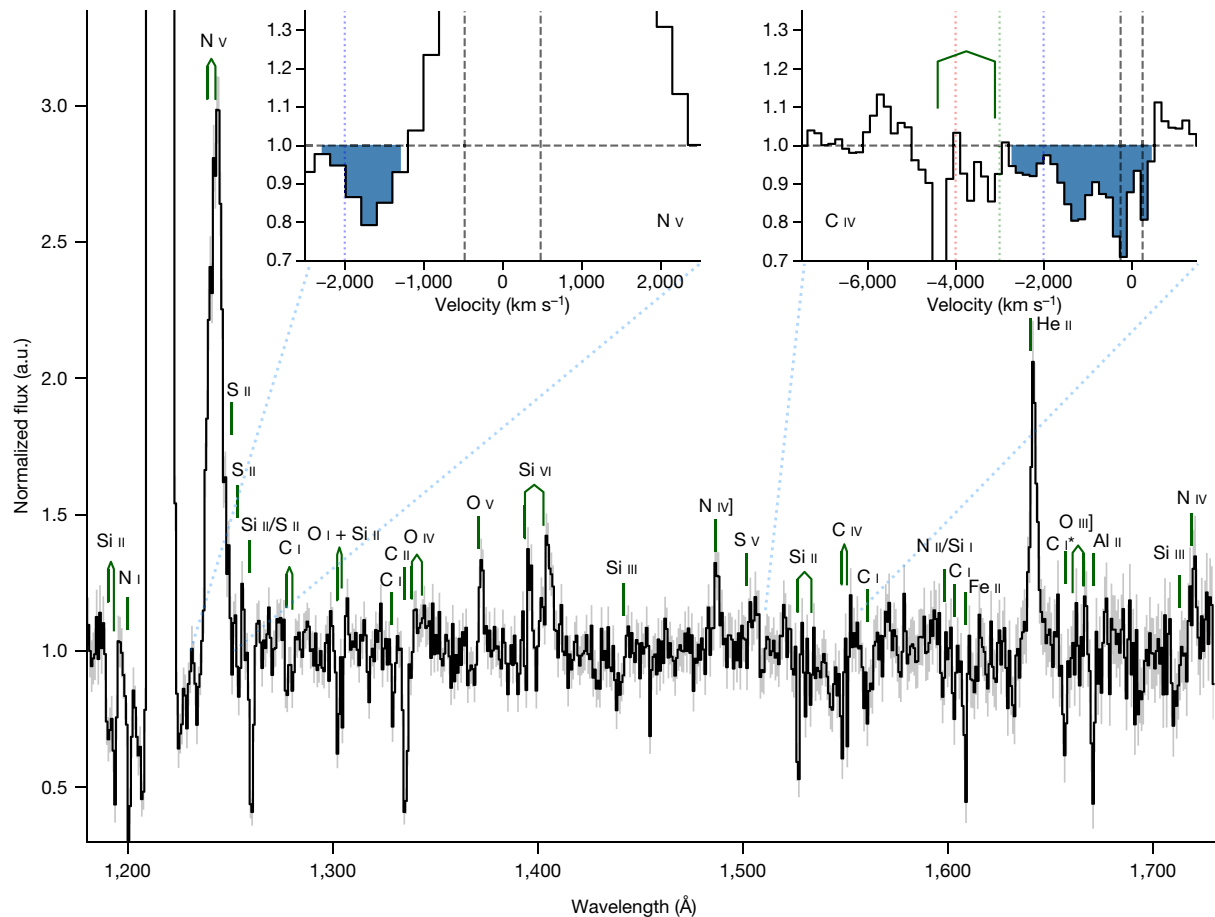
Fig. 3 | Average far-UV spectrum of Swift J1858.6−0814 during the luminous hard state. Numerous emission and absorption lines are present; the dominant transitions have been labelled with their corresponding rest position indicated with a green tick (semi-forbidden transitions are indicated with closing square brackets and excited atoms/ions with asterisks). All the emission components are skewed toward shorter wavelengths with blue absorption troughs, which are the characteristic footprint of disc outflows. Light grey areas represent the standard error. Insets, enlargements of the N v ($\lambda\lambda$1,284–1,437 Å) and C iv ($\lambda\lambda$1,513–1,668 Å) profiles with the blue-shifted absorption signatures highlighted in blue; in the latter the nearby Si ii interstellar absorption is indicated with connected green ticks. These signatures indicate the presence of a warm, moderately ionized accretion disc wind with characteristic velocities similar to those observed in the optical. a.u., arbitrary units.

The discovery of optical, UV and (probably) X-ray outflow signatures in the luminous hard state of J1858 suggests that disc winds may always be present in transient X-ray binaries, not just in disc-dominated soft states. Our identification of the constant (non-flaring) spectral component as the carrier of these signatures in the far-UV strongly supports this idea. X-ray and far-UV wind signatures have also been observed in some persistent soft-state X-ray binaries[26,27], that is, systems in which the disc is not subject to the instability that drives the outbursts of transient accretors[28].

The emerging physical picture of disc winds being an integral part of the accretion flows in X-ray binaries is consistent with theoretical modelling of outburst light curves[7,28]. It is also in line with radiation–hydrodynamical modelling of thermally driven outflows from X-ray binary discs[6,29,30]. These simulations confirm that strong mass loss is inevitable in any systems with a sufficiently large disc subject to strong irradiation, regardless of accretion state[6]. These conditions are met in J1858 (Methods). A key test of the thermally driven wind scenario will be to check that wind signatures are absent in systems in which these conditions are not met[31].

Regardless of the driving mechanism, two key outstanding questions are where and how these outflows manage to sustain a sufficiently low ionization state to enable the formation of optical and UV lines. The most likely answers are that self-shielding, probably coupled with clumping, protects parts of the dense base of the wind above the outermost disc regions from over-ionization. Indeed, recent hydrodynamical simulations of irradiated discs in active galactic nuclei predict the existence of clumpy, thermally unstable, multi-phase outflows[5]. This mechanism might also be at work in X-ray binaries, but new radiation–hydrodynamic simulations will be needed to confirm this.

Online content

Any methods, additional references, Nature Research reporting summaries, source data, extended data, supplementary information, acknowledgements, peer review information; details of author contributions and competing interests; and statements of data and code availability are available at https://doi.org/10.1038/s41586-021-04324-2.

1. Ponti, G. et al. Ubiquitous equatorial accretion disc winds in black hole soft states. *MNRAS* **422**, L11–L15 (2012).
2. Homan, J. et al. Evidence for simultaneous jets and disk winds in luminous low-mass x-ray binaries. *Astrophys. J.* **830**, L5 (2016).
3. Muñoz-Darias, T. et al. The changing-look optical wind of the flaring x-ray transient Swift J1858.6-0814. *Astrophys. J.* **893**, L19 (2020).
4. Long, K. S. & Knigge, C. Modeling the spectral signatures of accretion disk winds: a new Monte Carlo approach. *Astrophys. J.* **579**, 725–740 (2002).
5. Waters, T., Proga, D. & Dannen, R. Multiphase AGN winds from x-ray-irradiated disk atmospheres. *Astrophys. J.* **914**, 62 (2021).
6. Higginbottom, N. et al. Thermal and radiation driving can produce observable disc winds in hard-state X-ray binaries. *MNRAS* **492**, 5271–5279 (2020).
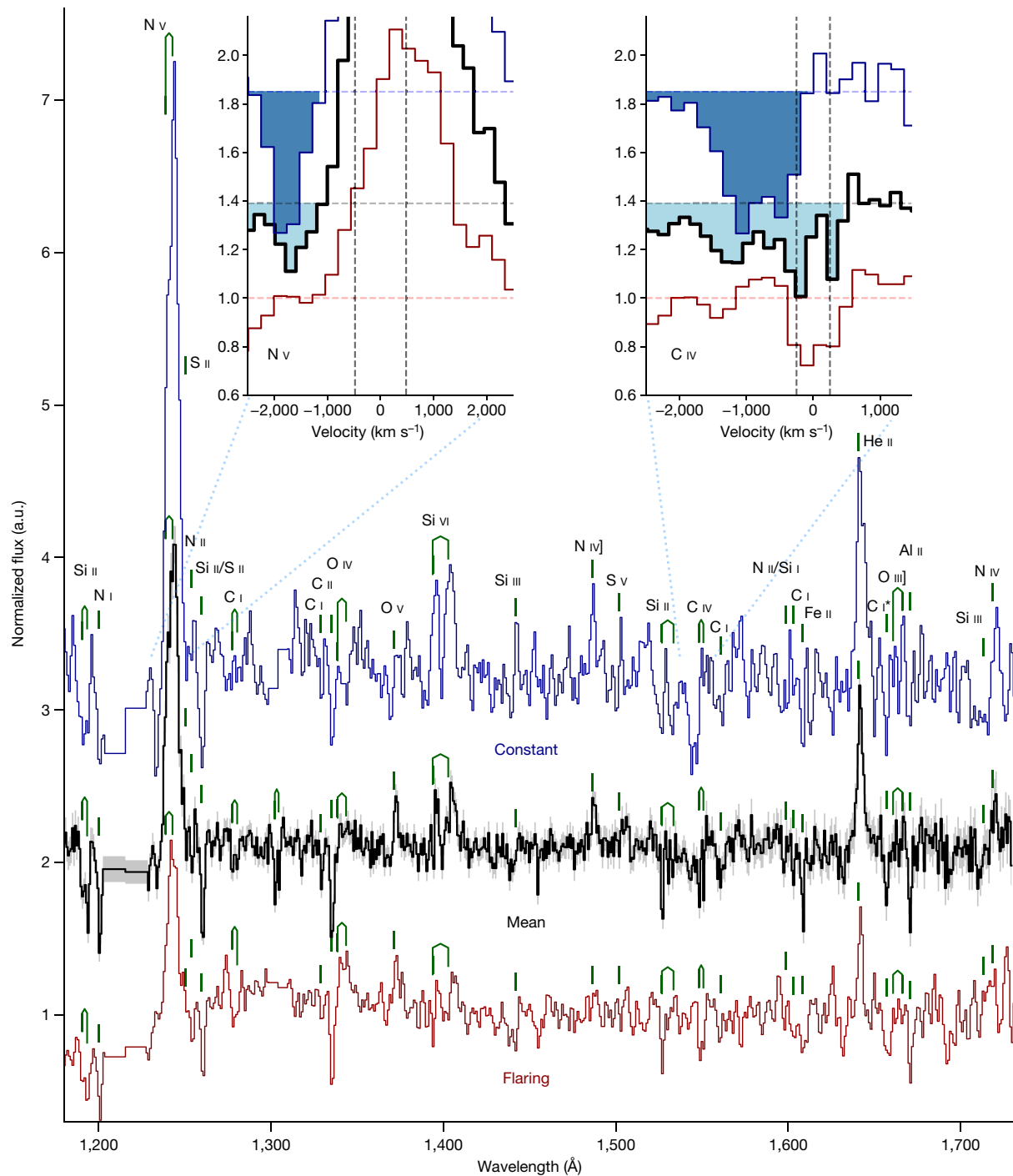
Fig. 4 | Spectral decomposition into a constant (blue) and flaring component (red). The flaring component is driven by the observed continuum variability in the far-UV. The average normalized spectrum is displayed with a thick black line for reference, and all are normalized to the continuum level. An offset has been added to the spectra for clarity. The regions of geocoronal emission such as Lyman α and Si II were removed to avoid artifacts in the spectral decomposition. Rest positions of the dominant ions are marked with a green tick and labelled in the top spectrum. Insets, enlargements of the two transitions in which the presence of the outflow is more prominent. Specifically, regions covered in the insets are $\lambda\lambda 1,284–1,474$ Å for N v and $\lambda\lambda 1,525–1,717$ Å for C IV.

7.   Tetarenko, B. E., Lasota, J. P., Heinke, C. O., Dubus, G. & Sivakoff, G. R. Strong disk winds traced throughout outbursts in black-hole X-ray binaries. *Nature* **554**, 69–72 (2018).

8.   Gehrels, N. et al. The Swift gamma-ray burst mission. *Astrophys. J.* **611**, 1005–1020 (2004).

9.   Krimm, H. A. et al. Swift reports the detection of a new galactic transient source Swift J1858.6-0814. *The Astronomer's Telegram* **12151**, 1 (2018).

10. Bright, J. et al. AMI-LA radio observations of the galactic X-ray transient Swift J1858.6-0814. *The Astronomer's Telegram* **12184**, 1 (2018).

11. Vasilopoulos, G., Bailyn, C. & Milburn, J. Swift J1858.6-0814: Localization and variability of the optical counterpart. *The Astronomer's Telegram* **12164**, 1 (2018).

12. Kennea, J. A. & Krimm, H. A. Swift J1858.6-0814: Swift XRT and UVOT localization. *The Astronomer's Telegram* **12160**, 1 (2018).

13. Buisson, D. J. K. et al. Discovery of thermonuclear (Type I) X-ray bursts in the X-ray binary Swift J1858.6-0814 observed with NICER and NuSTAR. *MNRAS* **499**, 793–803 (2020).

14. Buisson, D. J. K. et al. Dips and eclipses in the X-ray binary Swift J1858.6-0814 observed with NICER. *MNRAS* **503**, 5600–5610 (2021).

15. Ludlam, R. M. et al. Initial NICER observation of the new X-ray transient Swift J1858.6-0814. *The Astronomer's Telegram* **12158**, 1 (2018).

16. Motta, S. E. et al. Swift observations of V404 Cyg during the 2015 outburst: X-ray outflows from super-Eddington accretion. *MNRAS* **471**, 1797–1818 (2017).

17. Hare, J. et al. NuSTAR observations of the transient galactic black hole binary candidate Swift J1858.6–0814: a new sibling of V404 Cyg and V4641 Sgr? *Astrophys. J.* **890**, 57 (2020).

18. van den Eijnden, J. et al. The variable radio counterpart of Swift J1858.6-0814. *MNRAS* **496**, 4127–4140 (2020).

19. Begelman, M. C., McKee, C. F. & Shields, G. A. Compton heated winds and coronae above accretion disks. I. Dynamics. *Astrophys. J.* **271**, 70–88 (1983).

20. Done, C., Gierliński, M. & Kubota, A. Modelling the behaviour of accretion flows in X-ray binaries. Everything you always wanted to know about accretion but were afraid to ask. *Astron. Astrophys. Rev.* **15**, 1–66 (2007).

21. Higginbottom, N. & Proga, D. Coronae and winds from irradiated disks in x-ray binaries. *Astrophys. J.* **807**, 107 (2015).

22. Buisson, D. J. K. et al. Soft X-ray emission lines in the X-ray binary Swift J1858.6-0814 observed with XMM-Newton Reflection Grating Spectrometer: disc atmosphere or wind? *MNRAS* **498**, 68–76 (2020).

23. Muñoz-Darias, T. et al. Regulation of black-hole accretion by a disk wind during a violent outburst of V404 Cygni. *Nature* **534**, 75–78 (2016).

24. Shields, G. A., McKee, C. F., Lin, D. N. C. & Begelman, M. C. Compton-heated winds and coronae above accretion disks. III. Instability and oscillations. *Astrophys. J.* **306**, 90–106 (1986).

25. Ganguly, S. & Proga, D. On the wind-driven relaxation cycle in accretion disks. *Astrophys. J.* **890**, 54 (2020).

26. Ioannou, Z. et al. Understanding the LMXB X2127+119 in M 15. II. The UV data. *Astron. Astrophys.* **399**, 211–218 (2003).

27. Neilsen, J. et al. A NICER view of a highly absorbed flare in GRS 1915+105. *Astrophys. J.* **902**, 152 (2020).

28. Dubus, G., Done, C., Tetarenko, B. E. & Hameury, J.-M. The impact of thermal winds on the outburst lightcurves of black hole X-ray binaries. *Astron. Astrophys.* **632**, A40 (2019).

29. Luketic, S., Proga, D., Kallman, T. R., Raymond, J. C. & Miller, J. M. On the properties of thermal disk winds in x-ray transient sources: a case study of GRO J1655-40. *Astrophys. J.* **719**, 515–522 (2010).

30. Done, C., Tomaru, R. & Takahashi, T. Thermal winds in stellar mass black hole and neutron star binary systems. *MNRAS* **473**, 838–848 (2018).

31. Charles, P. et al. Hot, dense He II outflows during the 2017 outburst of the X-ray transient Swift J1357.2-0933. *MNRAS* **489**, L47–L52 (2019).

Article

Methods

Previous X-ray spectroscopy

Swift J1858.6−0814 was observed by XMM−Newton with the Reflection Grating Spectrometer (RGS) during March/April of 2019, a few months before the multi-wavelength campaign discussed in the present paper. A detailed analysis of XMM−Newton/RGS observations has already been presented elsewhere[22], so here we just briefly summarize some relevant results.

As it was during our campaign, Swift J1858.6−0814 was in a hard spectral state at the time of the XMM−Newton/RGS observations. In fact, there is no significant difference in the X-ray hardness ratios between the two epochs as seen by the all sky monitoring telescopes MAXI and Swift/BAT.

A search for wind signatures in the X-ray spectrum obtained with the RGS did not reveal any clear blue-shifted absorption features, which would be the 'smoking gun' for the presence of outflowing material. However, the N VII emission line is significantly red-shifted, which suggests that photons in the blue wing might be scattered out of our line of sight by an outflow. Thus, there is tentative evidence for an X-ray processing wind in the hard state from these observations. Assuming a neutron star with a typical mass of $1.4 M_\odot$, the velocity dispersion observed in this narrow line indicates that the bulk of the emission originated at $2-8 \times 10^9$ cm from the central source, consistent with the wind being thermally driven, as discussed below.

Finally, the absorbing column density inferred during its soft state is $N_H \simeq 2 \times 10^{21}$ cm^2, which is similar to the galactic extinction in the line of sight[13].

UV spectroscopy

Observations. Swift J1858.6−0814 was observed under the program GO/DD 15984 with N. Castro Segura as principal Investigator on 5 August 2019, 23:49:20 UT. A total of 4.9 ks exposure was obtained in the far-UV with the Cosmic Origin Spectrograph[32] and the G140L grating using the primary science aperture. This configuration provides a spectral resolution of $R = \lambda/\Delta\lambda \approx 900$, where λ is the wavelength. All the observations were obtained in TIME-TAG mode, yielding a stream of detected events at a time resolution of 32 ms.

Data analysis. We reduced the far-UV data using the HST CALCOS pipeline, provided by The Space Telescope Science Institute (https://github.com/spacetelescope). One-dimensional spectra were extracted using the TWOZONE algorithm, which sums over the cross-dispersion direction such that 99% of the flux is extracted at each wavelength. Errors are estimated from Poisson statistics, and the background is modelled with a smooth polynomial and subtracted from the target spectrum. We extracted light curves from the TIME-TAG event files using the same regions defined by the pipeline, except that empirical background correction was directly applied. Regions affected by geo-coronal airglow emission associated with Lyman α ($\lambda\lambda 1,208-1,225$ Å) and O II ($\lambda\lambda 1,298-1,312$ Å) were masked when extracting the light curves.

Spectral decomposition. The highly variable far-UV luminosity during our observations gives rise to a strongly bimodal logarithmic flux distribution (Extended Data Fig. 1). This is in line with the visual impression from the far-UV light curve that the dominant variability is due to 'shots' or 'flares' superposed on a roughly constant background (Fig. 1b).

We have isolated the spectra associated with these two components by carrying out a simple linear decomposition of our time-resolved spectroscopic data into a constant and a flaring (variable) component. Following ref. [33], we assume that the flux density $F(\lambda, t)$ at wavelength λ and time t can be written as

$$F(\lambda, t) = C(\lambda) + V(\lambda)D(t), \tag{1}$$

where $C(\lambda)$ and $V(\lambda)$ are the spectra of the constant and flaring components, respectively. The function $D(t)$ is the driving light curve of the flaring component.

To estimate $D(t)$, we constructed a far-UV continuum light curve at 10 s time resolution. We then estimated the underlying constant level in this light curve and created a normalized driving light curve from which this estimate was removed. We finally smoothed the resulting time series with a five-point, second-order Savitzky−Golay filter to obtain our estimate of $D(t)$. The result is shown as the red curve in Extended Data Fig. 2.

With $D(t)$ fixed, the decomposition described by equation (1) becomes just a series of N_λ two-parameter fits, where N_λ is the number of wavelength bins being considered. As the Cosmic Origin Spectrograph on HST uses a photon-counting far-UV detector, the dataset actually consists of a time- and wavelength-tagged event stream. Our decomposition is therefore based on an unbinned (in time) maximum likelihood fit to the data at the individual photon-event level, because this maximizes the signal-to-noise ratio of the inferred spectral components. The log-likelihood for this model can be derived from Poisson statistics and turns out to be

$$\ln \mathcal{L} \propto \left[\sum_{i=0}^{N_{phot}} \ln[\mathcal{C}(\lambda) + D(t)\mathcal{V}(\lambda)] \right] - \mathcal{N}. \tag{2}$$

Here $\mathcal{C}$ and $\mathcal{V}$ are now the count rates associated with the constant and variable components, N_{phot} and $\mathcal{N}$ are the total number of observed photons and those predicted by the model, respectively. We obtain best-fit estimates of $\mathcal{C}$ and $\mathcal{V}$ by maximizing equation (2). The flux-calibrated spectra, described as constant and flaring components in Fig. 4, are then constructed in the usual way, by multiplying by the wavelength-dependent inverse sensitivity curve. Detector regions dominated by background and/or geo-coronal emission are excluded from the fit.

Optical spectroscopy

During the HST visit, strictly simultaneous observations of Swift J1858.6−0814 were carried out with the X-Shooter[34] (program ID 2103.D-5052(A)) and OSIRIS[35] spectrographs (program ID GTC23-19A), mounted on the VLT UT2-Kueyen telescope in the Paranal Observatory and in the GTC at the Roque de los Muchachos Observatory, respectively. X-Shoooter yielded time-resolved optical/near-infra-red spectra covering the range $\lambda\lambda 0.3-2.4$ μm. With this instrument we obtained a total of 58 individual exposures with integration times of $\simeq 300$ s, for a total exposure time of $\simeq 17.4$ ks. We used slit widths of 0.9 and 1.0 arcsec in the UVB and visible, respectively, yielding corresponding velocity resolutions of approximately 51.33 km s^{-1}. The dataset was reduced using the standard European Southern Observatory (ESO)'s pipeline EsoReflex[36] version 3.3.5. Calibration frames were taken every 1 h and additionally during the occultation of HST by the Earth. A total of 20 science exposures each 5 min long were gathered with GTC/OSIRIS, covering the first 2 h of the campaign, using the grism R2500R ($\lambda\lambda 5,575-7,685$ Å) and one with R1000B ($\lambda\lambda 4,200-7,400$ Å), delivering a velocity resolution of approximately 160 km s^{-1} and 350 km s^{-1}, respectively. Further details on the data reduction of these observation are given in ref. [3].

Outflow diagnostics

The presence of blue-shifted absorption associated with far-UV and optical lines implies a significant column density of material in the lower level of the relevant atomic transition. This, in turn, can be used to set a rough lower limit on the mass-loss rate of the outflow.

Following ref. [37], we approximate the outflow as being spherical and adopt a simple Hubble-like $v \propto R$ velocity law. Combining the expression for the Sobolev optical depth with the continuity equation, the characteristic optical depth presented by such an outflow at velocity v in a given line can be written as

$$\tau \simeq 74.1 \left(\frac{f_{osc}}{0.2847}\right)\left(\frac{\lambda}{1,549.062 \text{ Å}}\right)\left(\frac{A}{7 \times 10^{-5}}\right)\left(\frac{f_{ion}}{1.00}\right)$$
$$\left(\frac{\dot{M}_{wind}}{10^{-10} \, M_\odot \, \text{yr}^{-1}}\right)\left(\frac{v}{1,500 \text{kms}^{-1}}\right)^{-2}\left(\frac{R(v)}{10^{10} \text{cm}}\right)^{-1}. \tag{3}$$

Here f_{osc} and λ are the oscillator strength and wavelength of the line, respectively, A is the abundance of the relevant element, f_{ion} is the fraction of those atoms in the correct ionization level, $\dot{M}_{wind}$ is the mass-loss rate of the outflow and $R(v)$ is the radius where velocity v is reached in the wind.

The reference values adopted for f_{osc}, λ and A in equation (3) are representative of the C IV resonance line (treated as a singlet). The reference velocity, $v \simeq 1,500$ km s^{-1}, is chosen based on the location of the blue-shifted absorption trough in the far-UV line profiles (Fig. 4). Our adopted value of $R(v) \simeq 10^{10}$ cm corresponds to the radius in the disc beyond which a thermally driven outflow is expected to be launched (see below); it is also roughly the radius where $v_{esc} \simeq 1,500$ km s^{-1}. Finally, by taking $f_{ion} = 1$, we ensure that our estimate of $\dot{M}_{wind}$ is a lower limit (modulo uncertainties in the other parameters).

On the basis of the depth of the absorption features in the far-UV line profiles, we expect that $\tau \gtrsim 1$ for both N V and C IV. The estimated lower limits on the mass-loss rates in units of solar mass per year are then $\dot{M}_{wind} \gtrsim 2 \times 10^{-11}$ from N V and $\dot{M}_{wind} \gtrsim 3 \times 10^{-12}$ from C IV. The larger of these numbers corresponds to a hydrogen column density of $N_H \simeq 2 \times 10^{19}$ cm^{-2}, if we adopt the same quasi-spherical wind model with an inner radius of 10^{10} cm. For comparison, a total column of $N_H \simeq 10^{24}$ cm^{-2} is required for the electron-scattering optical depth to reach $\tau_{es} \simeq 1$, as might be expected if the observed flaring is driven by time-dependent obscuration.

Is there a thermally driven disc wind in Swift J1858.6−0814?

The accretion discs in luminous X-ray binaries are subject to strong irradiation. As a result, the upper layers of the atmosphere can be heated to the inverse Compton temperature (T_{IC}), which depends only on the spectral energy distribution of the radiation field. The X-ray spectrum of Swift J1858.6−0814 in the hard state can be approximated as a power law with photon index $\Gamma = 1.5$ and an exponential cutoff at $E_{max} \simeq 30$ keV (ref. [22]). For such a spectrum, the Compton temperature is approximately $kT_{IC} \simeq E_{max}/12$ (where k is the Boltzman constant; ref. [38]), which gives $T_{IC} \simeq 3 \times 10^7$ K for Swift J1858.6−0814.

Mass loss from these heated layers is inevitable at radii at which the characteristic thermal speed of the ions, $v_{th} \simeq 3kT_{IC}/m_p$, exceeds the local escape velocity, $v_{esc} \simeq 2GM/R$; here, m_p is the proton mass, G is the gravitational constant and M is the mass of the compact object. Discs larger than the so-called Compton radius, $R_{IC} = (2GMm_n)/(3kT_{IC})$, are therefore expected to produce thermally driven outflows. For Swift J1858.6−0814, we obtain $R_{IC} \simeq 5 \times 10^{10}$ cm. In reality, the radius at which this mechanism turns on is typically $R_{min} \simeq 0.1R_{IC}$ (refs. [30,39,40]). In our mass-loss rate calculation above, we have adopted a characteristic radius $R \simeq 0.3R_{IC}$ for the line-forming region in the outflow.

The disc in Swift J1858.6−0814 is certainly large enough to drive such an outflow. The orbital period of the system is $P_{orb} \simeq 21.3$ h (ref. [14]). From Kepler's third law, and assuming a mass ratio $q = M_2/M_1 \lesssim 1$ (where M_1 and M_2 refer to the masses of the primary and the donor star, respectively), the binary separation is $a_{bin} \simeq 3 \times 10^{11}$ cm. If the disc is tidally limited, its outer radius will be roughly $R_{disc} \simeq 0.9R_1$, where R_1 is the Roche-lobe radius of the neutron star[41]. The outer disc radius is therefore expected to be $R_{disc} \simeq 1-2 \times 10^{11}$ cm, which is much larger than R_{IC}, let alone $R_{min} \simeq 0.1R_{IC}$.

The final condition for strong thermally driven mass loss is that the irradiating luminosity should be sufficiently strong, $L \gtrsim L_{crit} = 0.05L_{Edd}$ (ref. [19]). This is comparable to the time-averaged luminosity in the flaring hard state of Swift J1858.6−0814 (ref. [17]). It is therefore likely that the system is luminous enough to drive a powerful thermal disc wind.

Data availability

The data underlying this article are publicly available at https://archive.stsci.edu/hst/search.php program ID 15984 for HST/FUV data, http://archive.eso.org/cms.html program 190ID 2103.D-5052(A) for VLT/X-Shooter and https://gtc.sdc.cab.inta-csic.es/gtc/ program ID GTC23-19A for GTC/OSIRIS. X-ray data from NICER used all the OBSIDs starting with 120040, 220040, 320040 and 359201 accessible from HIESARC (https://heasarc.gsfc.nasa.gov/docs/nicer/nicer_archive.html). Source data are provided with this paper.

Code availability

Codes used for the analysis are available from the corresponding author upon reasonable request.

32. Green, J. C. et al. The Cosmic Origins Spectrograph. *Astrophys. J.* **744**, 60 (2012).
33. Eracleous, M. & Horne, K. The speedy magnetic propeller in the cataclysmic variable AE Aquarii. *Astrophys. J.* **471**, 427–446 (1996).
34. Vernet, J. et al. X-shooter, the new wide band intermediate resolution spectrograph at the ESO Very Large Telescope. *Astron. Astrophys.* **536**, A105 (2011).
35. Cepa, J. et al. In *Optical and IR Telescope Instrumentation and Detectors* Vol. 4008 of *Society of Photo-Optical Instrumentation Engineers (SPIE) Conference Series* (eds Iye, M. & Moorwood, A. F.) 623–631 (SPIE, 2000); https://doi.org/10.1117/12.395520
36. Freudling, W. et al. Automated data reduction workflows for astronomy. The ESO Reflex environment. *Astron. Astrophys.* **559**, A96 (2013).
37. Drew, J. E. Inclination and orbital-phase-dependent resonance line-profile calculations applied to cataclysmic variable winds. *MNRAS* **224**, 595–632 (1987).
38. Done, C. In *Accretion Processes in Astrophysics* (eds González Martínez-País, I., Shahbaz, T. & Casares Velázquez, J.) 184–227 (Cambridge Univ. Press, 2014).
39. Woods, D. T., Klein, R. I., Castor, J. I., McKee, C. F. & Bell, J. B. X-ray–heated coronae and winds from accretion disks: time-dependent two-dimensional hydrodynamics with adaptive mesh refinement. *Astrophys. J.* **461**, 767–804 (1996).
40. Proga, D. & Kallman, T. R. On the role of the ultraviolet and x-ray radiation in driving a disk wind in x-ray binaries. *Astrophys. J.* **565**, 455–470 (2002).
41. Frank, J., King, A. & Raine, D. J. *Accretion Power in Astrophysics* 3rd edn (Cambridge Univ. Press, 2002).
42. Ashman, K. M., Bird, C. M. & Zepf, S. E. Detecting bimodality in astrometrical datasets. *Astron. J.* **108**, 2348–2361 (1994).

Extended Data Fig. 1 | The logarithmic far-UV flux distribution of J1858 during our observations. The distribution is clearly bimodal, consistent with the visual impression from the light curve (Fig. 1b) of the variability being due to a flaring component that is superposed on a roughly constant component. The grey line is the optimal decomposition of the distribution into two Gaussians, as suggested by the KMM algorithm[42]. The blue and red lines correspond to the individual Gaussians. KMM rejects the null hypothesis of a single component with extremely high significance ($p < 10^{-43}$).
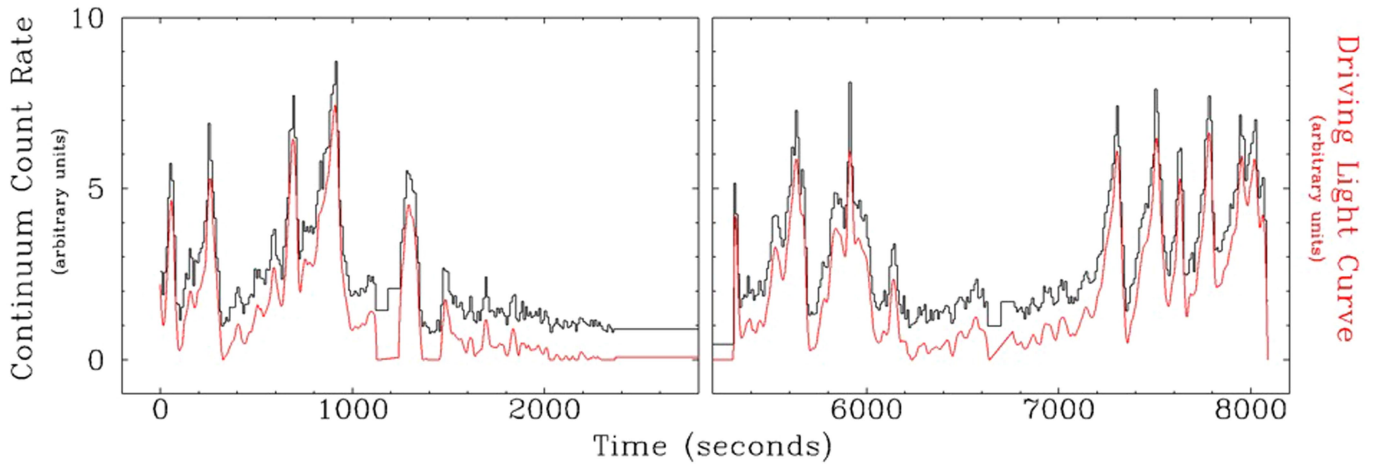
Extended Data Fig. 2 | The far-UV continuum and driving light curves. The black histogram shows the light curve of *Swift* J1858.6−0814 constructed from three broad wavelength regions that exclude the three strongest emission lines (N v λ1240, Si iv λ1400 and He ii λ1640). The specific regions used were $\lambda\lambda$1290 Å – 1390 Å, 1410 Å – 1630 Å, 1660 Å – 1850 Å. The light curve is shown normalized to an estimate of the underlying constant level (80 c s⁻¹).

The driving light curve used in the decomposition, $D(t)$, was constructed from this and is shown as the red curve. It was obtained by subtracting the estimate of the constant level, setting any slightly negative values to zero, and using a 5-point, 2nd order Savitzky-Golay filter to produce a slightly smoother, higher S/N version of the light curve.